Nanoscale

RSC Publishing

COMMUNICATION

View Article Online
View Journal | View Issue

Cite this: *Nanoscale*, 2013, **5**, 3664

Received 22nd January 2013
Accepted 13th March 2013

DOI: 10.1039/c3nr00369h

www.rsc.org/nanoscale

High responsivity, fast ultraviolet photodetector fabricated from ZnO nanoparticle–graphene core–shell structures

Dali Shao,*[a] Mingpeng Yu,[bc] Hongtao Sun,[b] Tao Hu,[b] Jie lian[b] and Shayla Sawyer[a]

We report a simple, efficient and versatile method for assembling metal oxide nanomaterial–graphene core–shell structures. An ultraviolet photodetector fabricated from the ZnO nanoparticle–graphene core–shell structures showed high responsivity and fast transient response, which are attributed to the improved carrier transport efficiency arising from graphene encapsulation.

As a wide band gap semiconductor material, ZnO has drawn a great deal of attention due to its unique optical and electrical properties including wide band gap (3.37 eV), large exciton binding energy (60 meV), and strong resistance to high energy proton irradiation.[1] In particular, various ZnO nanomaterials have been used for fabrication of ultraviolet (UV) photodetectors with high photoconductive gain and high responsivity.[2] Unfortunately, these UV photodetectors suffered poor transient response (up to minutes), which is attributed to surface defects and oxygen adsorption/desorption processes of ZnO nanomaterials. Therefore, it is very important to improve the transient response of ZnO nanomaterials for fast UV sensing. Methods using hydrogen doping and multiwalled carbon nanotube networks have been developed by our group to improve the transient response of ZnO nanowires (NWs)/p-Si heterojunction photodiodes.[3] However, further improvement of transient response of ZnO nanomaterials is still highly desirable for high performance UV photodetector applications.

Research on composite nanomaterials has attracted tremendous attention due to the possibility of multi-functional operation monolithically integrated on a single chip.[4] Graphene, as a novel carbon nanomaterial, has many remarkable material properties including high carrier transport mobility, large specific surface area, superior mechanical properties and excellent chemical stability.[5] The incorporation of graphene into the composites can provide them with the unique functions of graphene and also possibly induce intriguing properties inherited from synergetic effects.[6] Various graphene-based composite nanomaterials have been proved to be promising for a wide range of applications such as catalysis, optoelectronics, and energy conversion and storage devices.[7]

In this work, we used a simple method to wrap graphene onto ZnO NPs to fabricate high performance UV photodetectors with fast transient response and high responsivity. The synthesis procedure of the ZnO NP–graphene core–shell structure consists of three steps: surface modification of ZnO NPs with amine groups, coating of a graphene oxide (GO) shell on ZnO NPs, and conversion of the GO shell to graphene. Finally, ZnO NW–graphene, In_2O_3 NP–graphene and porous Co_2O_3 NP–graphene core–shell structures were synthesized as an illustration of the versatility of this method.

The ZnO NPs were synthesized using a wet chemical etching process and the details have been presented in our previous work.[8] An outline of the ZnO NP–graphene core–shell is shown

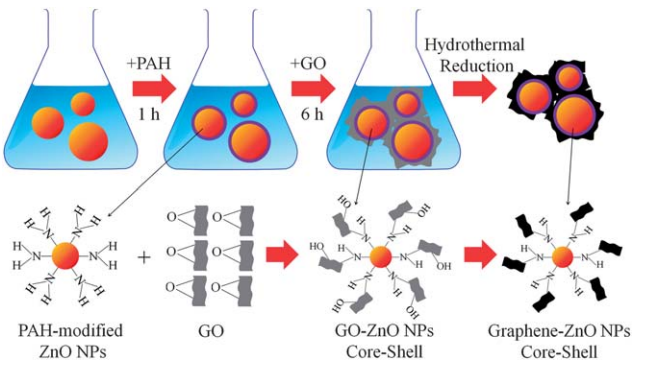

Fig. 1 Schematic illustration of the fabrication process for ZnO NP–graphene core–shell structures.

[a]*Department of Electrical, Computer and Systems Engineering, Rensselaer Polytechnic Institute, Troy, NY 12180, USA. E-mail: shaod@rpi.edu; Fax: +1-518-276-4403; Tel: +1-518-276-2164*

[b]*Department of Mechanical, Aerospace and Nuclear Engineering, Rensselaer Polytechnic Institute, Troy, NY 12180, USA*

[c]*College of Materials Science and Engineering, Key Laboratory of Advanced Functional Materials, Ministry of Education, Beijing University of Technology, Beijing 100022, China*

in Fig. 1, which is a modified method described by Zhou *et al.*[9] First, ZnO NPs were dipped into poly(allylamine hydrochloride) (PAH) solution for 1 h. The PAH solution is used to modify the surface of ZnO NPs by attaching amine groups. Second, the PAH-modified ZnO NPs were implanted in a GO dispersion. In this process, GO platelets are assembled onto the surface of PAH-modified ZnO NPs through two interactions: (1) the ring-opening reaction between the amine groups in the functionalized ZnO NPs and the epoxy groups in the GO platelets;[10] and (2) the electrostatic interaction between the positively charged amine-modified ZnO NPs and negatively charged GO platelets.[11] The GO platelets are able to cross-link the amine groups in the surface of PAH modified ZnO NPs *via* the epoxy groups of two or more platelets, stitching them together.[12] In conjunction with the electrostatic interaction, such a chemical cross-linking results eventually in the core–shell assembly between the ZnO NPs and GO platelets. Third, the resulting ZnO NP–GO core–shell was treated through a hydrothermal reduction process (at 180 °C for 20 h in an autoclave) aiming at transforming GO into graphene. Compared with the chemical reduction process that uses highly toxic and dangerous hydrazine (N_2H_4) as given in ref. 9, the hydrothermal reduction process in this work only needs water and no other pollutant will be introduced. In addition to being environment friendly, hydrothermal reduction process also have advantages such as technical convenience, high purity of the final product, low cost and high throughput.

A Carl Zeiss Ultra 1540 dual beam scanning electron microscope (SEM) was used to determine the size and morphology of the ZnO NP–graphene core–shell structure are shown in Fig. 2(a)–(c). The dimensions of the ZnO NPs core ranges from 100 to 150 nm. The ZnO NP–graphene core–shell structure was further examined by high resolution transmission electron microscopy (HRTEM, JEOL 2011) images shown in Fig. 2(d) and (e), from which the lattice spacing is determined to be ~2.6 Å, corresponding to the distance between the (0002) planes in the ZnO crystal lattice. The major Raman features of the ZnO NP–graphene core–shell structure are shown in Fig. 3(a), where the D band at around 1336 cm^{-1} and the G band at around 1590 cm^{-1} for the graphene shell were observed. The 2D band observed at around 2675 cm^{-1} has a very low intensity, which is likely attributed to the large amount of defects on the graphene shell. The relative intensity of the "disordered" D-band and the crystalline G-band (I_D/I_G) for the graphene shell is around 1.05. The XRD profile for the ZnO NP–graphene core–shell structure is presented in Fig. 3(b). The graphene shell has a broad (002) peak centered at around 21 degrees, corresponding to an interlayer spacing of 0.41 nm. The photoluminescence (PL) spectra and the UV-visible absorption spectra shown in Fig. 3(c) were measured using a Spex-Fluorolog-Tau-3 spectrofluorimeter and a Shimadzu UV-Vis 2550 spectrophotometer, respectively. The UV-visible absorption spectra of the ZnO NP–graphene core–shell structure have a cut-off wavelength at 375 nm, which is due to the band edge absorption of ZnO NPs. When excited at 330 nm, the PL spectrum of the ZnO NP–graphene core–shell structure shows two bands. The first band centered at 375 nm is from the band edge emission of ZnO NPs while the second band centered at 515 nm is the defect level emission due to the surface oxygen vacancies of the ZnO NPs.

A UV photodetector was fabricated by deposition of the ZnO NP–graphene core–shell onto the quartz substrate using a spin casting method. Then, interdigitated Al contacts with a thickness of 300 nm were deposited on the top of the ZnO NP–graphene thin film through an electron beam evaporation process. The schematic illustration of the fabricated UV photodetector is shown in Fig. 4(a).

The typical *I–V* characteristics of the photodetector were measured using a HP4155B semiconductor parameter analyzer in the dark and with UV illumination at 335 nm, as shown in Fig. 4(b). The photocurrent to dark current ratio at 20 V is approximately 600. The inset of Fig. 4(b) shows the dark current plotted in a linear scale, which demonstrates good ohmic contacts of this device. The transient response of the device shown in Fig. 4(c) was measured by turning on and turning off a UV light emitting diode with a peak wavelength at 335 nm. The inset of Fig. 4(c) shows an enlarged rising edge and falling edge of the transient response, from which the rise time and fall time

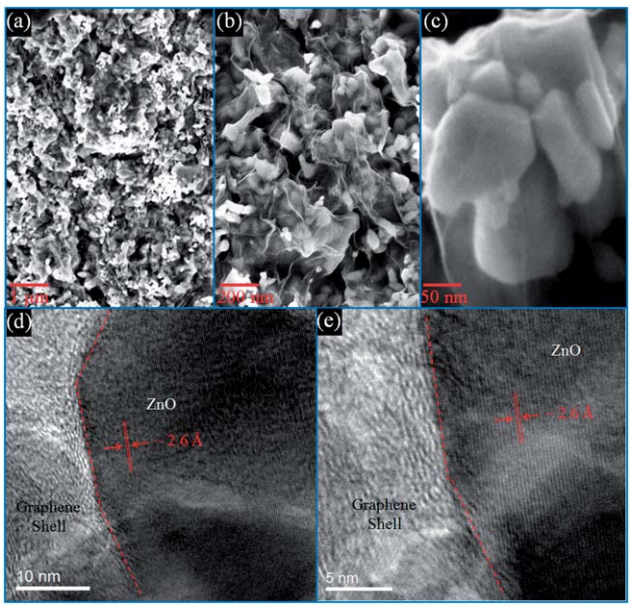

Fig. 2 (a–c) SEM images of ZnO NPs wrapped with graphene. (d and e) HRTEM images of ZnO NPs wrapped with graphene.

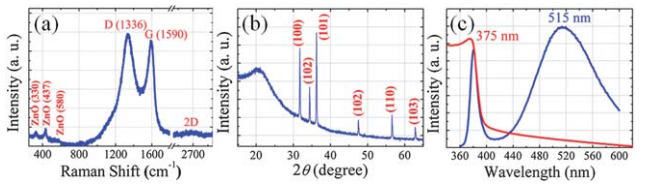

Fig. 3 (a) Raman spectra of ZnO NP–graphene core–shell structures. (b) XRD pattern of ZnO NP–graphene core–shell structures. (c) Absorption and PL spectra of ZnO NP–graphene core–shell structures.

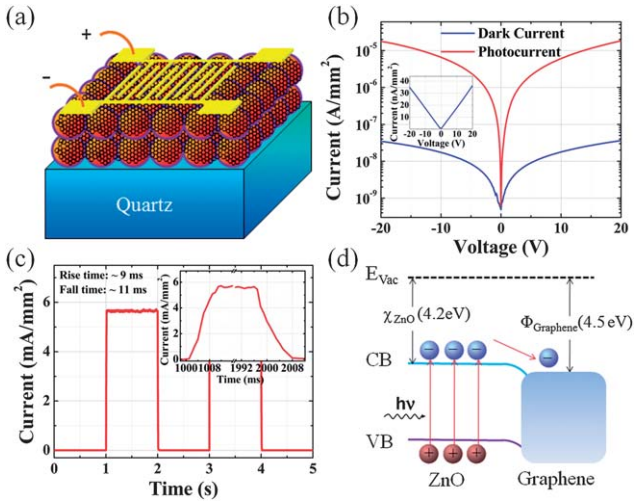

Fig. 4 (a) Schematic view of the UV photodetector fabricated from ZnO NP–graphene core–shell structures. (b) Typical *I–V* characteristics of the UV photodetector. Inset: linear scale plot of the dark current. (c) Transient response of the UV photodetector. Inset: enlarged rising and falling edge of the transient response. (d) Energy band alignment and carry transport mechanism of the ZnO NP–graphene core–shell composite.

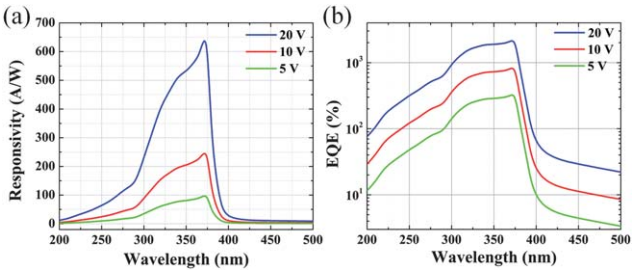

Fig. 5 (a) Photoresponsivity and (b) EQE of the UV photodetector fabricated from ZnO NP–graphene core–shell structures measured with varying bias voltages.

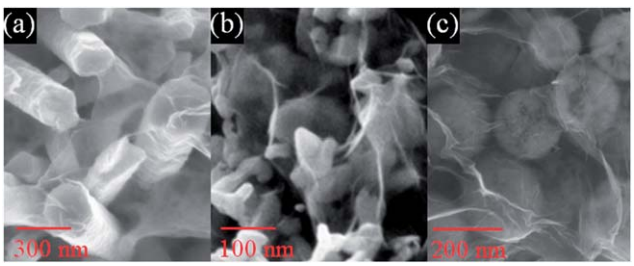

Fig. 6 High resolution SEM images of (a) ZnO NW–graphene, (b) In_2O_3 NP–graphene and (c) porous Co_2O_3 NP–graphene core–shell structures.

of the device were measured to be around 9 and 11 ms, respectively. This is at least three orders of magnitude faster than ZnO nanomaterials based UV photoconductors,[2] but still slower than UV photodetector fabricated from ZnO/GaN nanoscale p–n junctions (response time < 1 ms).[14] The fast transient response of the photodetector in this work can be understood from the carrier transport process and energy band diagram of the ZnO NP–graphene core–shell structure shown in Fig. 4(d). The electron affinity for ZnO is 4.2 eV and the work function of the graphene sheet is known to be 4.5 eV below the vacuum level.[13] Thus, when ZnO is in contact with the graphene, it is energetically favorable for the photogenerated electrons to get transferred from the conduction band of ZnO to the graphene. Since graphene has high carrier mobility, less accumulation of the electrons on the graphene side is expected. Therefore, the carrier transport efficiency can be effectively improved in the core–shell structure, leading to a fast rise in the photocurrent. When UV illumination is turned off, the excess electrons in the graphene are transferred to the ZnO side for recombination with holes which is a very fast process, thus a fast decay was observed for the ZnO NP–graphene core–shell structure. It is worth mentioning that fast UV response was also observed for a graphene–ZnO nanowire–graphene vertical sandwich structure, in which the Schottky barrier between graphene and ZnO NWs contributed to the fast transient response.[15]

The photoresponsivity of the device (shown in Fig. 5), defined as photocurrent per unit of incident optical power, was measured by a Shimadzu UV-Vis 2550 spectrophotometer with a deuterium lamp (190–390 nm) and a halogen lamp (280–1100 nm). A maximum photoresponsivity 640 A W^{-1} at 375 nm was observed under 20 V bias, which is lower than the responsivity of the metal–semiconductor–metal UV photodetector fabricated from ZnO NPs in our previous work (731.42 A W^{-1}).[8b] The decrease of responsivity in this work may be attributed to the reduced amount of hole trapping states (negative charged oxygen ions) on the surface of ZnO NPs after graphene encapsulation.[2] Fig. 5(b) shows the external quantum efficiency (EQE) of the photodetector calculated using the equation: EQE = $R \times h\nu$, where $h\nu$ is the energy of the incident photon in electronvolts and R is the photoresponsivity of the UV photodetector.

It is important to note that the method for wrapping graphene onto ZnO NPs presented in this work is a general strategy which can also be applied to various metal oxide nanomaterials. To examine the versatility of this method, ZnO NW–graphene, In_2O_3 NP–graphene and porous Co_2O_3 NP–graphene core–shell structures were synthesized. The high resolution SEM images of ZnO NW–graphene, In_2O_3 NP–graphene and porous Co_2O_3 NP–graphene core–shell structures are shown in Fig. 6(a)–(c), respectively. The ZnO NW–graphene and the In_2O_3 NP–graphene core–shell structures were synthesized for UV photodetector applications. The porous Co_2O_3 NP–graphene core–shell structure was used for high performance energy storage applications and the results will be presented in another work.

Conclusions

A general strategy is applied to achieve the self-assembled wrapping of graphene sheets around ZnO NPs, ZnO NWs, In_2O_3 NPs and porous Co_2O_3 NPs. The UV photodetector fabricated from ZnO NP–graphene core–shell structures showed fast transient response and high photoresponsivity, which are attributed to improved structural integrity and carrier transport efficiency through graphene encapsulation. In addition to the ZnO NP–graphene core–shell structure, ZnO NW–graphene,

In_2O_3 NP–graphene and porous Co_2O_3 NP–graphene core–shell structures were synthesized as an illustration of the versatility of the method presented in this work, which may have high potential for future optoelectronics and energy storage applications.

Acknowledgements

The authors gratefully acknowledge support from National Security Technologies through NSF Industry/University Cooperative Research Center Connection One. The authors also acknowledge the National Science Foundation Smart Lighting Engineering Research Center (EEC-0812056) and a NSF career award DMR 1151028.

Notes and references

1 (*a*) C.-Y. Chang, F.-C. Tsao, C.-J. Pan, G.-C. Chi, H.-T. Wang, J.-J. Chen, F. Ren, D. P. Norton, S. J. Pearton, K.-H. Chen and L.-C. Chen, *Appl. Phys. Lett.*, 2006, **88**, 173503; (*b*) D. C. Look, C. Coskun, B. Claflin and G. C. Farlow, *Phys. Rev. B: Condens. Matter Mater. Phys.*, 2003, **32**, 340–342.

2 (*a*) C. Soci, A. Zhang, B. Xiang, S. A. Dayeh, D. P. R. Aplin, J. Park, X. Y. Bao, Y. H. Lo and D. Wang, *Nano Lett.*, 2007, **7**, 1003–1009; (*b*) Y. Jin, J. Wang, B. Sun, J. C. Blakesley and N. C. Greenham, *Nano Lett.*, 2008, **8**, 1649–1653; (*c*) S.-M. Peng, Y.-K. Su, L.-W. Ji, C.-Z. Wu, W.-B. Cheng and W.-C. Chao, *J. Phys. Chem. C*, 2010, **114**, 3204–3208; (*d*) L. Guo, H. Zhang, D. Zhao, B. Li, Z. Zhang, M. Jiang and D. Shen, *Sens. Actuators, B*, 2012, **166**, 12–16.

3 (*a*) D. Shao, M. Yu, J. Lian and S. Sawyer, *Appl. Phys. Lett.*, 2012, **101**, 211103; (*b*) D. Shao, M. Yu, J. Lian and S. Sawyer, *Appl. Phys. Lett.*, 2013, **102**, 021107.

4 (*a*) J. Liu, J. Jiang, C. Cheng, H. Li, J. Zhang, H. Gong and H. J. Fan, *Adv. Mater.*, 2011, **23**, 2076–2081; (*b*) W. Zhou, C. Cheng, J. Liu, Y. Y. Tay, J. Jiang, X. Jia, J. Zhang, H. Gong, H. H. Hng, T. Yu and H. J. Fan, *Adv. Funct. Mater.*, 2011, **21**, 2439–2446.

5 (*a*) S. Watcharotone, D. A. Dikin, S. Stankovich, R. Piner, I. Jung, G. H. B. Dommett, G. Evmenenko, S. E. Wu, S. F. Chen, C. P. Liu, S. T. Nguyen and R. S. Ruoff, *Nano Lett.*, 2007, **7**, 1888–1892; (*b*) L. A. Ponomarenko, F. Schedin, M. I. Katsnelson, R. Yang, E. W. Hill, K. S. Novoselov and A. K. Geim, *Science*, 2008, **320**, 356–358; (*c*) X. Wang, L. Zhi and K. Mullen, *Nano Lett.*, 2008, **8**, 323–327; (*d*) C. O. Girit, J. C. Meyer, R. Erni, M. D. Rossell, C. Kisielowski, L. Yang, C. H. Park, M. F. Crommie, M. L. Cohen, S. G. Louie and A. Zettl, *Science*, 2009, **323**, 1705–1708; (*e*) A. K. Geim and K. S. Novoselov, *Nat. Mater.*, 2007, **6**, 183–191.

6 (*a*) J. Liu, J. Jiang, C. Cheng, H. Li, J. Zhang, H. Gong and H. J. Fan, *Adv. Mater.*, 2011, **23**, 2076–2081; (*b*) W. Zhou, C. Cheng, J. Liu, Y. Y. Tay, J. Jiang, X. Jia, J. Zhang, H. Gong, H. H. Hng, T. Yu and H. J. Fan, *Adv. Funct. Mater.*, 2011, **21**, 2439–2446.

7 (*a*) C. Peng, B. W. Jiang, Q. Liu, Z. Guo, Z. J. Xu, Q. Huang, H. J. Xu, R. Z. Tai and C. H. Fan, *Energy Environ. Sci.*, 2011, **4**, 2035–2040; (*b*) K. K. Manga, J. Wang, M. Lin, J. Zhang, M. Nesladek, V. Nalla, W. Ji and K. P. Loh, *Adv. Mater.*, 2012, **24**, 1697–1702; (*c*) S. W. Hwang, D. H. Shin, C. O. Kim, S. H. Hong, M. C. Kim, J. Kim, K. Y. Lim, S. Kim, S.-H. Choi, K. J. Ahn, G. Kim, S. H. Sim and B. H. Hong, *Phys. Rev. Lett.*, 2010, **105**, 127403; (*d*) H. L. Li, S. P. Pang, S. Wu, X. L. Feng, K. Mullen and C. Bubeck, *J. Am. Chem. Soc.*, 2011, **133**, 9423–9429; (*e*) Y. C. Qiu, K. Y. Yan, S. H. Yang, L. M. Jin, H. Deng and W. S. Li, *ACS Nano*, 2010, **4**, 6515–6526.

8 (*a*) L. Qin, C. Shing, S. Sawyer and P. S. Dutta, *Opt. Mater.*, 2011, **33**, 359–362; (*b*) L. Qin, C. Shing and S. Sawyer, *IEEE Electron Device Lett.*, 2011, **32**, 51–53.

9 W. Zhou, J. Zhu, C. Cheng, J. Liu, H. Yang, C. Cong, C. Guan, X. Jia, H. J. Fan, Q. Yan, C. M. Li and T. Yu, *Energy Environ. Sci.*, 2011, **4**, 4954–4961.

10 H. Bai, C. Li and G. Shi, *Adv. Mater.*, 2011, **23**, 1089–1115.

11 T. H. Han, W. J. Lee, D. H. Lee, J. E. Kim, E.-Y. Choi and S. O. Kim, *Adv. Mater.*, 2010, **22**, 2060–2064.

12 J. Oh, J. H. Lee, J. C. Koo, H. R. Choi, Y. Lee, T. Kim, N. D. Luong and J. D. Nam, *J. Mater. Chem.*, 2010, **20**, 9200–9204.

13 (*a*) L. J. Brillson and Y. Lu, *J. Appl. Phys.*, 2011, **109**, 121301; (*b*) G. Giovannetti, P. A. Khomyakov, G. Brocks, V. M. Karpan, J. van den Brink and P. J. Kelly, *Phys. Rev. Lett.*, 2008, **101**, 026803.

14 Y.-Q. Bie, Z.-M. Liao, H.-Z. Zhang, G.-R. Li, Y. Ye, Y.-B. Zhou, J. Xu, Z.-X. Qin, L. Dai and D.-P. Yu, *Adv. Mater.*, 2011, **23**, 649–653.

15 X.-W. Fu, Z.-M. Liao, Y.-B. Zhou, H.-C. Wu, Y.-Q. Bie, J. Xu and D.-P. Yu, *Appl. Phys. Lett.*, 2012, **100**, 223114.